POLITECNICO DI TORINO
Repository ISTITUZIONALE

Efficient Analytical Design Strategy for High-Gain Nonresonant Partially-Reflective-Surface Antennas

(Article begins on next page)

20 July 2025

Submitted to IEEE Antennas and Wireless Propagation Letters. Confidential until published

Efficient Analytical Design Strategy for High-Gain Non-Resonant Partially-Reflective-Surface Antennas

Xiaodong Zheng, Yuehe Ge, *Senior Member, IEEE*, Guowei Li, *Student Member, IEEE*, Ziheng Zhou, *Member, IEEE*, Ladislau Matekovits, *Senior Member, IEEE*, and Zhizhang (David) Chen, *Fellow, IEEE*

Abstract—**Non-resonant partially reflective surface (PRS) antennas (PRSAs) offer high-gain performance, but their design typically requires extensive electromagnetic simulations to obtain near-field phase distributions, leading to time-consuming processes, especially for complex or large antennas. This paper presents a novel analytical design method that significantly simplifies the design of phase-correcting surfaces (PCSs) for non-resonant PRSAs. By introducing a new design strategy based on a ray-tracing approach, we derive a set of analytical formulas for two PCS configurations: one utilizing a single superstrate that integrates both PRS and PCS functionalities, and another employing distinct PRS and PCS layers. Using these formulas, we designed two non-resonant PRSAs, and both simulated and experimental results demonstrate comparable gain performance to those obtained using Ansys HFSS. This approach reduces the dependence on computationally intensive simulations, offering a more efficient pathway for the design of high-performance non-resonant PRSAs, thereby advancing the accessibility and practicality of antenna design methodologies.**

Index Terms—**Partially reflective surface (PRS), non-resonant PRS antenna; ray-tracing method, phase-correcting surface (PCS).**

I. INTRODUCTION

High-gain, low-profile, and easily integrable antennas are crucial for creating efficient, compact platforms for modern and future wireless communication systems. Partially reflective surface (PRS) antennas (PRSAs) have emerged as a candidate for such applications due to their simple design, simple structure, low cost, and ease of integration. The study of PRS antennas dates back to the 1950s [1]. However, it was only with the advent of electromagnetic (EM) bandgap structures [2] and metasurfaces [3] that PRS antennas have garnered significant attention from researchers over the past two decades [4], [5], [6], [7], [8], [9], [10], [11], [12], [13], [14], [15], [16]. Despite this renewed interest, most research on PRS antennas has remained tied to the resonant conditions proposed in their early development [1], rendering these antennas resonant in nature.

Recently, non-resonant PRSAs have been introduced [17], utilizing metasurface phase-correcting surfaces (PCSs) to mitigate the out-of-phase leakage waves generated by the non-resonant cavity, thereby achieving improved high-gain radiation performance. These antennas demonstrate significantly enhanced peak gain and gain bandwidth compared to their resonant counterparts. However, the design process for non-resonant PRSAs involves intricate challenges, particularly the need for precise knowledge of the near-field distribution at the PRS to effectively design the PCS and optimize gain performance. This adds considerable complexity to the antenna design process, requiring the use of computationally intensive three-dimensional (3D) EM simulation tools, especially for large or complex PRSA designs.

This paper introduces a novel analytical design method for non-resonant PRSAs, based on the fundamental working principles of PRS cavity antennas [1], [17] and the metasurface nature of PCSs [3], [18]-[22]. By establishing clear operating principles and a design strategy, we utilize a ray-tracing approach to develop an innovative analytical methodology. This enables efficient, straightforward design of non-resonant PRSAs, similar to resonant designs, but without the need for time-consuming 3D EM simulations. Our method allows for rapid and accurate design of PCSs, greatly simplifying the overall design process and reducing the computational burden, thereby advancing the practical application of non-resonant PRSAs.

II. THE PROPOSED RAY-TRACING FORMULAS FOR THE DESIGN OF NON-RESONANT PRSAs

A. Proposed Operating principle and Design Strategy

The schematic diagram of a typical PRSA is shown in Fig. 1. It consists of a fully reflective ground (GND), a PRS, and a small center-fed feeding antenna on the GND. Ideally, the EM waves inside the cavity between the PRS and GND, excited by the center-fed feeding antenna, will partially radiate through the PRS while also propagating radially within the cylindrical cavity. It is assumed that the leaky waves on the PRS's top and

X. Zheng, Y. Ge, G. Li, and Z. Zhou are with the College of Physics and Information Engineering, Fuzhou University, Fuzhou 350108, China. (email: 1219583507@qq.com; yuehe@ieee.org; 852353758@qq.com; zhouzh@fzu.edu.cn).

L. Matekovits is with the Department of Electrical and Telecommunication, Politecnico di Torino, 10129 Torino, Italy, also with the Istituto di Elettronica e di Ingegneria dell'Informazione e delle Telecomunicazioni, National Research Council of Italy, 10129 Turin, Italy, and also with Politehnica University Timișoara, 300006 Timișoara, Romania. (email: ladislau.matekovits@polito.it).

Z. Chen is with the Department of Electrical and Computer Engineering, Dalhousie University, Halifax, NS B3H 4R2, Canada. (email: zz.chen@ieee.org)

bottom surfaces, centered at point O (the center of the PRS), have identical amplitudes and phases. For example, EM waves at points (r_2, θ_0) and (r_2, θ_1) as shown in Fig. 1, are considered to have the same amplitude and phase characteristics. This assumption simplifies the 3D analysis of the PRSA to a 2D cross-sectional examination through the center O.
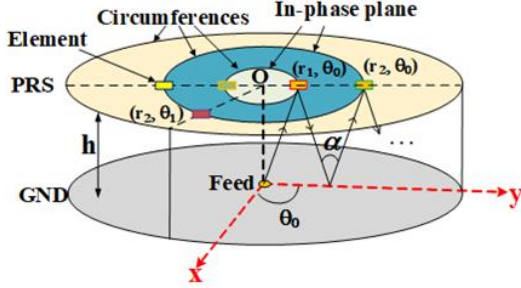

Fig. 1. Schematic of a typical (resonant and non-resonant) PRSA.

As detailed in the foundational paper on PRSAs [1], ray-tracing analysis leads to the established resonant condition for designing high-gain resonant PRSAs. However, this resonant condition is not applicable to the newly developed non-resonant PRSAs [17]. In these antennas, the EM waves on the top surface of the PRS are out of phase, preventing the waves from focusing and achieving high-gain performance. In our previous work [17] on non-resonant PRSA designs, we introduced a PCS above the PRS to correct the phases of incoming EM waves, aligning them in phase. To accomplish this, it is necessary to know the phases of the EM waves on the top or bottom surfaces of the PRS. These phases cannot be directly or analytically obtained through EM theory and must be calculated using 3D EM simulation software. Once these phases are determined, the corresponding correcting phases can be computed, and the PCS can be designed.

In practical applications, the PCS functions as an artificial 2D material composed of multiple periodic or aperiodic elements. According to Huygens's principle [23], [24], the PCS can be viewed as an antenna array, where each element of the PCS acts as an individual antenna element. The radiation performance of the PCS can be assessed by analyzing the equivalent array, with each array element being excited by rays reaching its center. In this section, we consider two different non-resonant PRSA scenarios and derive efficient analytical design formulas for them.

B. Non-Resonant PRSA with a Combined PRS/PCS

Fig. 2(a) illustrates the schematic diagram of a non-resonant PRSA, which includes a PEC GND, a center-fed feed, and a superstrate. This superstrate serves a dual function, acting both as the PRS and the PCS. The superstrate (PRS/PCS) is a metasurface, composed of discrete elements that can have different reflection phases (φ_i) and controllable transmission phases (ψ_i). To estimate the phases (Θ_i) of the EM waves on the bottom surface of the PRS, only the rays reaching the centers of the PRS elements are considered. The angle α can be determined by the period of the PRS and the cavity height (h). According to the typical ray-tracing analysis [1], the phase Θ_i of ray i on the bottom surface of the PRS can be expressed as:

$$\Theta_1 = -\frac{2\pi}{\lambda}\frac{h}{\cos(\frac{\alpha}{2})} + \beta_0 \qquad (1)$$

$$\Theta_2 = -\frac{2\pi}{\lambda}\frac{3h}{\cos(\frac{\alpha}{2})} - \pi + \varphi_1 + \beta_0 \qquad (2)$$

$$\Theta_i = -\frac{2\pi}{\lambda}\frac{(2i-1)h}{\cos(\frac{\alpha}{2})} - (i-1)\pi + \sum_{j=1}^{i-1}\varphi_j + \beta_0 \qquad (3)$$

where λ is the operating wavelength, h is the cavity height, α is angle between ray i and normal to the GND, as shown in Fig. 2(a), and β_0 denotes the initial phase of the EM wave emitted from the feed. Using Formulas (1)-(3), the phases Θ_i on the bottom surface of each PRS element can be determined. The transmission phases ψ_i, which also serve as the compensation or correcting phases, can then be computed from Θ_i. This enables the design of the superstrate that combines the functionalities of both the PRS and PCS. The phases of the EM waves on the top surface of each PRS element can be obtained by $\phi_i = \Theta_i + \psi_i$. By appropriately designing ψ_i on the PRS/PCS superstrate, all the ϕ_i values will be similar. Consequently, the EM waves on the top surface of the PRS/PCS superstrate will be in phase, resulting in a high-gain pencil radiation beam on the broadside of the non-resonant PRSA.
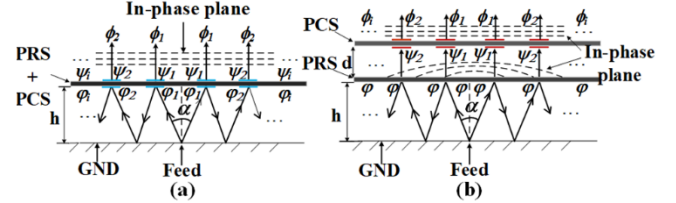

Fig. 2. Non-Resonant PRSA: (a) with a combined PRS/PCS superstrate; (b) with separate PRS and PCS layers.

C. Non-Resonant PRSA with separate PRS and PCS

In Fig. 2(b), a non-resonant PRSA with a different configuration is depicted, utilizing two separate superstrates: a PRS and a PCS. The PRS is partially reflective, with a uniform reflection phase, φ, across its entire surface, as indicated in Fig. 2(b). The PCS, which has a periodic structure, fully transmits the incoming EM waves, and each PCS element provides a tunable transmission phase, ψ_i. In the ray-tracing analysis, it is assumed that the EM wave passes through the center of each element, as shown in Fig. 2(b). The phase (ϕ_i) on the top surface of each PCS element can be expressed as follows:

$$\phi_i = (i-1)\varphi - \frac{2\pi}{\lambda}\frac{(2i-1)h}{\cos(\frac{\alpha}{2})} - (i-1)\pi + \psi_i \qquad (4)$$

Based on the assumption that the EM waves on the PRS or PCS elements along the concentric circle have the same amplitude and phase, the compensation phases required for designing the PCS in the two non-resonant PRSA configurations illustrated in Fig. 2 can be calculated analytically using Formulas (1)-(4).

On a two-dimensional surface of the PRS or PCS, the centers of discrete elements may not always align with concentric circles whose radii are integer multiples of the PRS or PCS period. To estimate the phase Θ_i for elements not situated on these concentric circles, one can first calculate the phases for the two nearest concentric circles. Subsequently, Θ_i can be approximated by using the phase corresponding to the nearest concentric circle or by averaging the phases from the two

nearest concentric circles.

III. DESIGNS OF LP/CP NON-RESONANT PRSAs FOR VALIDATION

In this section, we present the design of two non-resonant PRSAs aiming at validating the proposed efficient method in Section II.
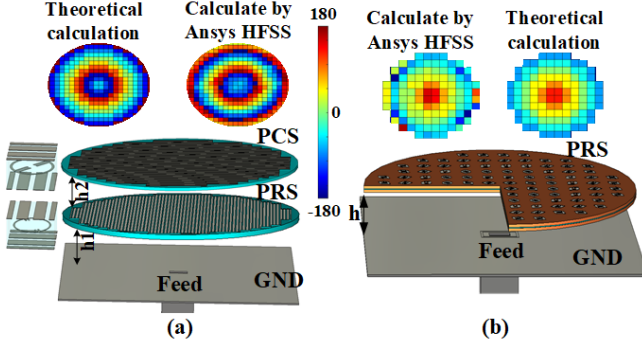

Fig. 3. The concerned non-resonant PRSA configurations and the phase distributions on the bottom surfaces of the PRS: (a) with separate PRS and PCS; (b) with a single superstrate combining the functionalities of the PRS and PCS.

A. Non-Resonant PRSA Design with Separate PRS and PCS

Fig. 3(a) displays a linearly polarized (LP) non-resonant PRSA design at 12.5 GHz, consisting of separate PRS and PCS components. The center feed is a standard WR-75 open waveguide. Both the PRS and PCS utilize the same metasurface [18], [19], [20], with the element design depicted in the figure. Consequently, the PRS and PCS share a period of 6mm (0.25λ at 12.5 GHz). The Fabry-Perot (FP) metasurface element independently controls transmission amplitude and phase [19]. In this design, the PRS maintains uniform reflection amplitude and phase, while the PCS achieves nearly 100% transmission amplitude with tunable phases. Metasurface element parameters at 12.5 GHz are referenced from [20]. Eight FP elements are used to construct the PRS and PCS.

The phase distribution on the PRS surface is initially calculated using Formulas (1)-(3), yielding the phases of the EM waves on the bottom PRS surface at the centers of each PCS element. These phase values inform the compensation phases required for PCS design using the eight FP metasurface elements [20]. The main parameters of the PRSA design in Fig. 3(a) are as follows: h=15mm (0.625λ at 12.5 GHz), d=3mm (0.125λ), and D=132mm. Both the PRS and PCS comprise 384 FP metasurface elements.

To validate the design, ANSYS HFSS was used for comparison. The phase distributions on the bottom PRS surface, obtained from both Formulas (1)-(3) and ANSYS HFSS, are plotted in Fig. 3(a). Similar phase distributions are observed in the central regions, with discrepancies in the outer regions.

Simulations using Ansys HFSS were performed for validation of three PRSA designs: PRSA1, PRSA2, with PCSs obtained via the proposed method and HFSS, respectively, and PRSA3 without a PCS. All designs share a cavity height (h) of 0.625λ, making them non-resonant at 12.5 GHz.

Directivity results are shown in Fig. 4(a). PRSA1 and PRSA2

exhibit similar peak directivities at 12.5 GHz, while PRSA3 shows significantly lower directivity due to the absence of a PCS. Though PRSA2 shows better gain bandwidth, PRSA1's directivity underscores the efficiency of the proposed analytical design method. Fig. 4(b) illustrates the reflection coefficients, indicating that the presence of a PCS influences the impedance matching of the open waveguide.
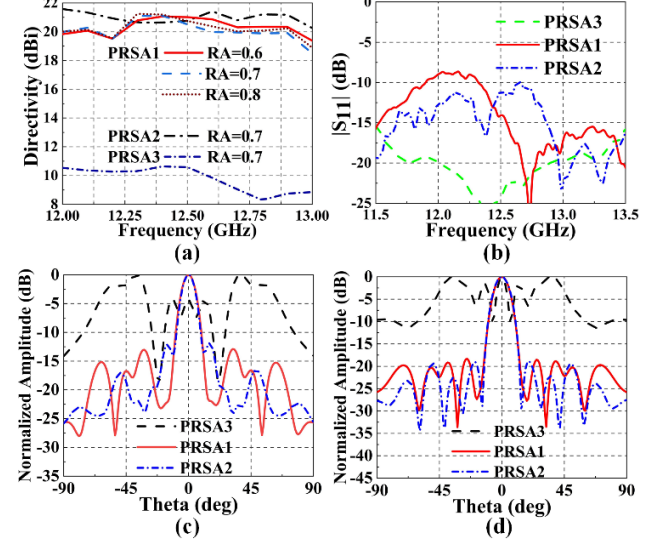

Fig. 4. The simulated results for PRSA1, PRSA2, and PRSA3: (a) directivities, where RA denotes the uniform reflection amplitude of the PRS; (b) |S₁₁|; (c) radiation patterns at 12.5 GHz in the E plane; (d) radiation patterns at 12.5 GHz in the H plane.

Radiation patterns at 12.5 GHz in the E and H planes are depicted in Fig. 4(c) and (d). PRSA3 shows abnormal patterns due to the non-resonant antenna cavity, while PRSA1 and PRSA2 produce well-formed pencil beams.

These simulations confirm that high-gain non-resonant PRSAs, as configured in Fig. 3(a), can be effectively designed using the proposed analytical method.

B. Non-Resonant PRSA Design with a Single Superstrate

Next, a compact circularly polarized (CP) non-resonant PRSA operating at 12.5 GHz is designed, as shown in Fig. 3(b). A single superstrate integrating both PRS and PCS functionalities is developed using periodically arranged metasurface elements, depicted in Fig. 5(a). These elements, previously used in transmitarray antennas [21], [22], provide high gain and linear-to-circular polarization (LP-CP) conversion. In this design, they are re-engineered for partial reflectivity while maintaining LP-CP conversion and transmission phase compensation.

The PRS/PCS superstrate consists of two identical F4BTM dielectric substrates (εr=2.94, loss tangent=0.0015) bonded with a thin FR4 film. Each superstrate element comprises two U-slot patches: the bottom patch acts as the receiver, and the top patch as the transmitter. The element converts LP EM waves into CP EM waves. Element parameters are detailed in Fig. 5(a), with final design values listed in Table I.

Characterization of the PRS/PCS element was performed using Ansys HFSS under LP incidence on the Rx patch. Fig. 5(b) shows the reflection amplitudes and phases for eight

4

Submitted to IEEE Antennas and Wireless Propagation Letters. Confidential until published

elements with identical dimensions but varying Tx patch rotation angles. The reflection amplitudes are approximately 0.8, with nearly identical phases. Fig. 5(c) illustrates the transmission phases, showing a linear progression with a uniform $45°$ step, and axial ratios demonstrating LP-CP conversion with values below 3 dB at 12.5 GHz.

Table I
Parameter values of the PRS/PCS elements (unit: mm)

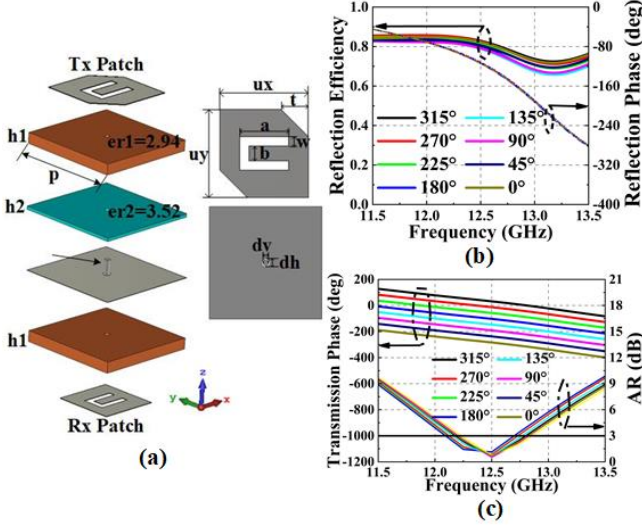| p	h1	h2	ux	uy	a	b	w	t	dv	dh
12	1.27	0.36	5.8	5.8	3.2	1	0.6	1.8	0.6	0.9

Fig. 5. (a) Configuration of the concerned metasurface element; (b) Reflection efficiency and phases; (c) Transmission phases and axial ratios.
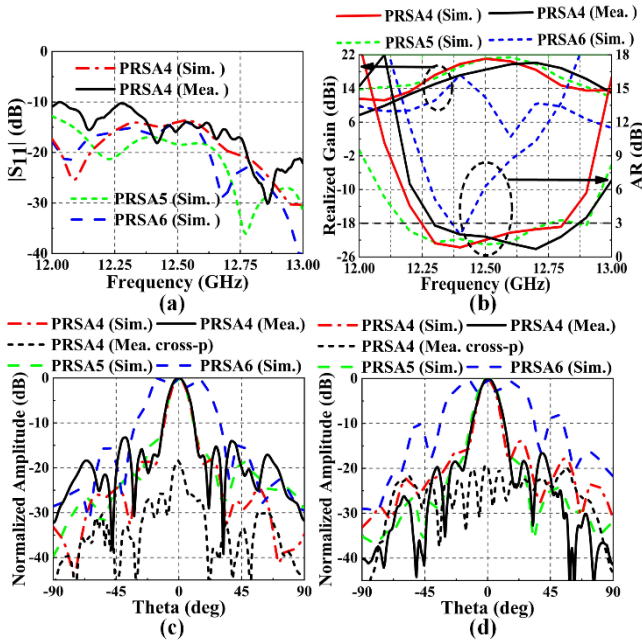

Fig. 6. The simulated and measured results for PRSA4, PRSA5, and PRSA6: (a) $|S_{11}|$; (b) gains and axial ratios; (c) radiation patterns at 12.5 GHz in the E plane; (d) radiation patterns at 12.5 GHz in the H plane.

A CP non-resonant PRSA, based on the elements in Fig. 5, is designed to operate at 12.5 GHz, using the configuration in Fig. 3(b). The superstrate, functioning as both PRS and PCS, has an element period of 12 mm (0.5λ) and a cavity height of 0.6λ. The circular superstrate, 156 mm in diameter (6.5λ), contains 112 elements. A standard WR-75 open waveguide is used as the

feed at the center of the GND.

The non-resonant CP PRSAs, denoted as PRSA4 and PRSA5, were designed using Formulas (1)-(3) and Ansys HFSS, respectively. PRSA6 shares the same parameters as PRSA4 but without performing the phase compensation. These PRSA designs were first simulated with Ansys HFSS, followed by the fabrication and mounting of PRSA4, which was subsequently measured in an anechoic chamber.

Fig. 6 compares the simulated and measured results. All three designs show reflection coefficients below -10 dB, with PRSA4 and PRSA5 demonstrating high gain and superior 3-dB axial ratios compared to PRSA6, which exhibited abnormal performance. PRSA4's simulated peak gain is 21 dBi, with a measured peak gain of 20.3 dBi; the corresponding aperture efficiencies are 30.2% and 25.7%. The results agree well, with discrepancies attributed to measurement noise, fabrication inaccuracies, and assembly errors.

In Fig. 6(c) and (d), radiation patterns for the three antennas are illustrated. The measured results for PRSA4 are reasonable, validating our proposed efficient design method for non-resonant PRSAs.

Table II Comparison among different PRSAs and this work

Ref.	Ant. type	Ant. height	Gain (dBi)	GBW (3-dB)	3-dB AR BW
[17]	non-resonant	1.16λ	25.3	9.2%	
[25]	Resonant	1λ	17.2	5.7%	>4%
[26]	Resonant	0.58λ	13.7	13.8%	>8.6%
Our work (Fig. 3(a))	non-resonant	1λ	20.1	8.4%	
Our work (Fig. 3(b))	non-resonant	0.75λ	20.3	3.6%	3.8%

Table II compares our PRSAs with previously reported resonant and non-resonant designs. While the resonant PRSA without a PCS [4], [12] have a lower profile, non-resonant PRSAs offer higher peak gains and aperture efficiencies at the cost of slightly increased antenna heights and narrower bandwidths.

V. Conclusion

This paper presents a novel and efficient method for designing non-resonant PRSAs. By introducing new design strategy and applying the ray-tracing method, we successfully derived analytical formulas to compute the phase compensation required for PCSs. This approach enables the efficient design of PRSAs while significantly reducing the reliance on time-intensive electromagnetic simulations. Two non-resonant PRSAs with distinct PRSA/PCS configurations were designed and validated through both simulations and experiments. The results confirm the effectiveness of our method, highlighting its ability to simplify the design process with minimal impact on performance, thus offering a practical and time-saving solution for the development of advanced PRSAs.

References

[1] G. V. Trentini, "Partially reflecting sheet arrays," *IEEE Trans. Antennas Propag.*, vol. 4, pp. 666–671, Oct. 1956.

5

Submitted to IEEE Antennas and Wireless Propagation Letters. Confidential until published

[2]   M. Thevenot, C. Cheype, A. Reineix, and B. Jecko, "Directive photonic-bandgap antennas," *IEEE Trans. Microw. Theory Techn.*, vol. 47, no. 11, pp. 2115-2122, Nov. 1999.

[3]   C. L. Holloway, E. F. Kuester, J. A. Gordon, J. O'Hara, J. Booth, and D. R. ZSmith, "An overview of the theory and applications of metasurfaces: the two-dimensional equivalents of metamaterials," *IEEE Antenna & Propag. Mag.*, vol. 54, no. 2, pp. 10-35, April 2012.

[4]   A. P. Feresidis and J. C. Vardaxoglou, "High gain planar antenna using optimized partially reflective surfaces," *IEE Proc. Microw., Antennas Propag.*, vol. 148, no. 6, pp. 345–350, Dec. 2001.

[5]   Y. Ge, K. P. Esselle, and Y. Hao, "Design of low-profile high-gain EBG resonator antennas using a genetic algorithm," *IEEE Antennas Wireless Propag. Lett.*, vol. 6, pp. 480–483, 2007.

[6]   Y. Ge, K. P. Esselle, and T. S. Bird, "The use of simple thin partially reflective surfaces with positive reflection phase gradients to design wideband, low-profile EBG resonator antennas," *IEEE Trans. Antennas Propag.*, vol. 60, no. 2, pp. 743-750, Feb. 2012.

[7]   K. Konstantinidis, A. P. Feresidis, and P. S. Hall, "Dual subwavelength Fabry-Perot cavities for broadband highly directive antennas," *IEEE Antennas Wireless Propag. Lett.*, no. 13, pp. 1184 – 1186, 2014.

[8]   Y. Ge, and C. Wang, "A millimeter-wave wideband high-gain antenna based on Fabry-Perot resonator antenna concept," *Progress in Electromagnetic Research C*, vol. 50, pp. 103-111, 2014.

[9]   Y. Ge, Z. Sun, Z. Chen, and Y.-Y. Chen, "A high-gain wideband low-profile Fabry–Pérot resonator antenna with a conical short horn," *IEEE Antennas Wireless Propag. Lett.*, vol. 15, pp. 1889–1892, 2016.

[10] F. Costa, D. Bianchi, A. Monorchio, and G. Manara, "Linear Fabry-Perot/leaky-wave antennas excited by multiple sources," *IEEE Trans. Antennas Propagat.*, vol. 66, no. 10, pp. 5150–5159, Oct. 2018.

[11] A. Lalbakhsh, M. U. Afzal, K. P. Esselle, and S. L. Smith, "Wideband near-field correction of a Fabry–Pérot resonator antenna," *IEEE Trans. Antennas Propag.*, vol. 67, no. 3, pp. 1975–1980, Mar. 2019.

[12] N. Wang, Q. Liu, C. Wu, L. Talbi, Q. Zeng, and J. Xu, "Wideband Fabry-Perot resonator antenna with two complementary FSS layers," *IEEE Trans. Antennas Propag.*, vol. 69, no. 5, pp. 2463–2471, Feb. 2021.

[13] D. Comite, S. K. Podilchak, M. Kuznetcov, V. G. Buendia, P. Burghignoli, P. Baccarelli, and A. Galli, "Wideband array-fed Fabry-Perot cavity antenna for 2-D beam steering," *IEEE Trans. Antennas Propag.*, vol. 69, no. 2, pp. 784–794, Feb. 2021.

[14] P. Xie, G. Wang, and X. Zou, "Gain and AR improvements of the wideband circularly polarized Fabry-Perot resonator antenna," *IEEE Trans. Antennas Propag.*, vol. 69, no. 10, pp. 6965-6970, Oct. 2021.

[15] M. Y. Jamal, M. Li, K. L. Yeung, X. Li, L. Jiang, and T. Itoh, "A low-profile Fabry-Perot cavity antenna using anisotropic metasurface," *IEEE Antennas Wireless Propag. Lett.*, vol. 21, no. 2, pp. 356–360, Feb. 2022.

[16] A. Chatterjee, K. Dutta, S. Chakrabarti, and R. Mitta, "Advanced design of high-gain Fabry-Perot cavity antenna offering wide common impedance and gain bandwidth," *IEEE Antennas Wireless Propag. Lett.*, vol. 22, no. 5, pp. 1214–1218, May 2023.

[17] X. Ren, Y. Ge, and Z. Chen, "A partially reflecting surface antenna with a non-resonant cavity and a phase-correcting surface for gain enhancement," *IEEE Trans. Antennas Propag.*, vol. 71, no. 2, pp. 1244-1253, Feb. 2023.

[18] D. Y. Liu, M. H. Li, X. M. Zhai, L. F. Yao, and J. F. Dong, "Enhanced asymmetric transmission due to Fabry-Perot-like cavity," *Opt. Express*, vol. 22, no. 10, pp. 11707-11712, 2014.

[19] Y. Wang, Y. Ge, Z. Chen, X. Liu, J. Pu, K. Liu, H. Chen, and Y. Hao, "Broadband high-efficiency ultrathin metasurfaces with simultaneous independent control of transmission and reflection amplitudes and phases," *IEEE Trans. Microw. Theory Techn.*, vol. 70, no. 1, pp. 254–263, Jan. 2022.

[20] G. Li, Y. Ge, and Z. Chen, "A compact multibeam folded transmitarray antenna at Ku-band," *IEEE Antennas Wireless Propag. Lett.*, vol. 20, no. 5, pp. 808–812, May 2021.

[21] F. Diaby, A. Clemente, K. T. Pham, R. Sauleau, and L. Dussopt, "Circularly polarized transmitarray antennas at Ka-band," *IEEE Antennas Wireless Propag. Lett.*, vol. 17, no. 7, pp. 1204-1208, Jul. 2018.

[22] J. Wang, Y. Ge, Z. Chen, Z. Chu, J. Chen, Z. Zhou, and Z. Xu, "Compact wideband circularly-polarized mechanically beam-steering antenna for Ka-band vehicular communications", *IEEE Trans. Veh. Technol.*, vol. 73, no. 3, pp. 3393-3402, March 2024.

[23] V. H. Rumsey, "Some new forms of Huygens' principle", *IRE Transaction on Antennas Propagation*, vol. 7, no. 5, pp. 103–116, 1959.

[24] Z. Wang, S. Lin, Y. Ge, Z. Chen, J. Zhao, J. Chen, Z. Zhou, and T. S. Bird, "Unlock the potential of large-element-spacing arrays: a meta-lens solution for grating-lobe suppression and gain enhancement," *Electromagnetic Science*, Accepted. doi: 10.23919/emsci.2024.0030.

[25] Y.-L. Li and K.-M. Luk, "Dual circular polarizations generated by selfpolarizing Fabry–Pérot cavity antenna with loaded polarizer," IEEE Trans. Antennas Propag., vol. 69, no. 12, pp. 8890–8895, Dec. 2021.

[26] H. D. Le, T. Le-Huu, K. K. Nguyen and S. X. Ta, "Dual Circularly Polarized Fabry–Perot Antenna Using Single-Layer Self-Polarizing PRS," *IEEE Antennas Wireless Propag. Lett.*, vol. 22, no. 10, pp. 2575-2579, Oct. 2023.